JOURNAL OF SOLID STATE CHEMISTRY 114, 575–584 (1995)

$Tl_2Nb_2O_{6+x}$ ($0 \leq x \leq 1$): A Continuous Cubic Pyrochlore Type Solid Solution

J. L. Fourquet, H. Duroy, and Ph. Lacorre

Laboratoire des Fluorures, URA CNRS 449, Faculté des Sciences, Université du Maine, Avenue O. Messiaen, 72017 Le Mans Cedex, France

Received April 20, 1994; in revised form June 29, 1994; accepted July 8, 1994

Thallium metaniobate, $Tl_2Nb_2O_6$, belongs to the cubic pyrochlore structural type (space group *Fd3m*). It is demonstrated by TGA, chemical analysis, and X-ray thermodiffractometry that it gives a continuous solid solution $Tl_2Nb_2O_{6+x}$ ($0 \leq x \leq 1$) under oxidation; the cubic pyrochlore structure is maintained with a continuous decreasing unit cell edge: x oxide ions being progressively incorporated into the network while x Tl^{3+} ions substitute to x Tl^{+} ones. Rietveld refinements of X-ray powder diffraction data reveal that, in the classical model of the pyrochlore structure, Tl^{+} and Tl^{3+} are disordered on half of the 32*e* positions for $0 \leq x < 0.5$ and on the 16*d* ones for $0.5 < x \leq 1$. Bond valence calculations are in good agreement with the decrease in the splitting of Tl cations from 32*e* to 16*d* positions when x increases, provided that a correlation exists between oxygen insertion and the Tl^{3+} distribution: each extra oxygen O′ oxidizes one of its closest Tl neighbors to +3 while the three remaining monovalent Tl cations are repelled.

INTRODUCTION

Cubic $Tl_2Ta_2O_6$ was first discovered by Vorres (1). Belyaev *et al.* (2) pointed out that the $TlNbO_3$ X-ray powder diffraction pattern was very similar to that of cubic natural pyrochlore; they showed (3) that the $Tl_2M_2O_{6+x}$ series (M = Nb, Ta) can be obtained by thermal decomposition of hydrated niobate or tantalate. Ramadass *et al.* (4) found that $Tl_2Nb_2O_{6.6}$ and $Tl_2Ta_2O_{6.8}$ are formed when Tl_2CO_3 and M_2O_5 (M = Nb, Ta) are heated in air at 700°C. Michel (5) showed that $Tl_2Nb_2O_6$ heated in air at 600°C gives a black cubic pyrochlore $Tl_2Nb_2O_{6.2}$. All these observations are consistent with the existence of the series $Tl_2M_2O_{6+x}$ (M = Nb, Ta) but their extent and their crystal structure are not exactly known as yet.

This paper is devoted to the description of the synthesis and the study of the crystal structure of the $Tl_2Nb_2O_{6+x}$ series for $0 \leq x \leq 1$.

1. PREPARATION AND THERMAL CHARACTERIZATION OF THE $Tl_2Nb_2O_{6+x}$ SERIES

As previously described, nominal $Tl_2Nb_2O_6$ can be prepared by heating a stoichiometric mixture of Tl_2CO_3 and Nb_2O_5, under primary vacuum or inert atmosphere, first at 300°C for 6 hr and then at 550°C for 10 hr according to the reaction scheme

$$Tl_2CO_3 + Nb_2O_5 \rightarrow Tl_2Nb_2O_6 + CO_2.$$

Under these conditions, a clear brown and homogeneous, well-crystallized and single-phased cubic pyrochlore is obtained.

$Tl_2Nb_2O_{6+x}$ compositions are produced by oxidation, at pO_2 = 1 bar, of nominal $Tl_2Nb_2O_6$. The scheme of the oxidation process was thought to be

$$Tl_2^{+}Nb_2O_6 + x/2\ O_2 \rightarrow Tl_{2-x}^{+}Tl_x^{3+}Nb_2O_{6+x}.$$

TGA measurements (Perkin–Emer TGS2 apparatus, O_2 flow) were made in order to confirm the oxygen absorption. In the first experiment, 83.4 mg of nominal $Tl_2Nb_2O_6$ was heated 2.0°C/min by successive steps (150, 350, 450, 550°C) so that the sample stayed at the same temperature for 2 hr; under these conditions, a small progressive weight increase with a maximum gain at 450°C was observed. The total $\Delta m/m$ was 0.5%, compared to 2.32% calculated for $x = 1$. In another experiment, the saturated phase, obtained at the end of the first run, was slowly cooled from 550 to 50°C at 1.5°C/min; no weight change was observed, so it was concluded that the reaction process proposed above is not reversible.

Prolongated heating for 10 hr allows an increase of the oxidation range. Black cubic pyrochlore single phases were produced but with smaller unit cell parameters than those of the nominal $Tl_2Nb_2O_6$. After an HCl solution attack, the Tl^{+} content of the different samples was classically determined by redox potentiometric titration with $NaBrO_3$ solutions. It was found that, under pO_2 = 1 bar, the limit of the pyrochlore solid solution was $Tl_{1.35}^{+}Tl_{0.65}^{3+}Nb_2O_{6.65}$.

In an effort to increase the x value, oxidation under oxygen pressure was attempted. Two experiments were performed at 350°C on pelletized samples, in a furnace inserted in a Nova Swiss pressure vessel. They led to the

0022-4596/95 $6.00

following results after 2 hr under 13 bar O_2, x was found to be 0.90 ± 0.05, and after 24 hr under 150 bar O_2, x reached 1.09 ± 0.05.

All the compositions were stable when left at room temperature in ambient atmosphere.

For each sample, the unit cell edge of the cubic pyrochlore was refined by a least-squares fit from X-ray powder diffraction data (Cu$K\alpha$ monochromated) obtained with a PW1380 Philips goniometer equipped with DACO MP. Figure 1 presents the variation in the unit cell edge length over the composition range. It can be seen that it is not easy to synthesize pure—i.e., Tl^{3+}-free—$Tl_2Nb_2O_6$ and that the oxidation process—substitution of x Tl^+ by x Tl^{3+} and concomitant insertion of x oxide ions in the network—produces a significant and continuous shortening of the a parameter; this will be discussed in the Structural Study section. The oxidation process was also followed by X-ray thermodiffractometry (O_2 flow) on a Siemens D5000 θ/θ diffractometer (Co$K\alpha$) equipped with an Elphyse position-sensitive detector and an Anton Parr temperature attachment. The temperature was raised (12°C/min) by steps of 10°C from 30 to 500°C; the sample was then cooled to room temperature by the same procedure, with a diffraction pattern being recorded at each-

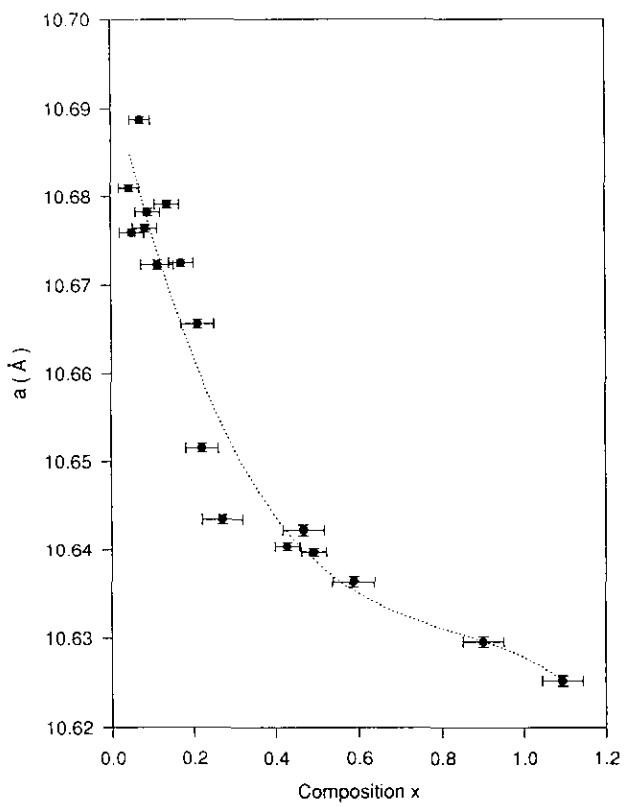

FIG. 1. Evolution of the unit cell edge length versus composition (the dotted line is a visual guide).

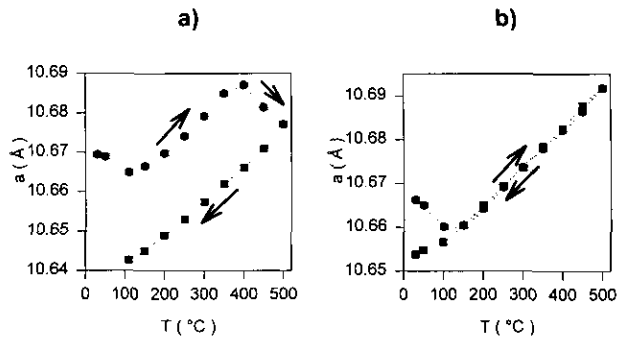

FIG. 2. Evolution of the unit cell edge length versus temperature during the thermodiffractometry experiments (under pO_2 = 1 bar (a), and under He atmosphere (b)); the dotted line is a visual guide).

temperature step. Figure 2 presents the evolution of the unit cell edge length versus temperature: from 30 to 400°C, the increase in a results from the fact that up to this temperature, the thermal expansion is greater than the shortening caused by the oxidation process. From 400 to 500°C, a decreases; we can assume that, in this temperature range, the oxidation process is predominant–as shown by the TGA study—over the thermal expansion. From 500°C to room temperature, the unit cell edge then decreases linearly to a value shorter than that of the starting material. The previous assumption has been checked by performing thermodiffractometry experiments under He atmosphere; they show almost no decrease of the a parameter after the same thermal cycle (Fig. 2). The slight contraction observed at low increasing temperature is probably due to the absorption of residual oxygen in the chamber.

2. STRUCTURAL STUDY

$Tl_2Nb_2O_6$ belongs to the $A_2B_2O_6\square$ defect cubic pyrochlore family; the composition of the normal pyrochlore is $A_2B_2O_6O'$. In the classical model (space group $Fd3m$, symmetry center at the origin, $Z = 8$, $a \cong 10$ Å), A ions are located in 16d positions $(\frac{1}{2}, \frac{1}{2}, \frac{1}{2})$, B ions in 16c positions (0, 0, 0), O anions in 48f $(v, \frac{1}{8}, \frac{1}{8})$, and O′ in 8$b$ positions $(\frac{3}{8}, \frac{3}{8}, \frac{3}{8})$.

The $A_2B_2O_6\square$ defect cubic pyrochlore family is represented by $Ag_2Sb_2O_6$ (6), $Pb_2Ru_2O_6$ (7), and $Bi_2Rh_2O_6$ (8). Many compounds are found resulting from a progressive filling of the 8b centered cages of the network, thus leading to the $A_2B_2O_6O'_x$ formulation, e.g., $Tl_2Ru_2O_{7-\delta}$ (9), $Pb_2B_2O_{7-\delta}$ (B = precious metal) (10).

The pyrochlore structure has been frequently described: it is built up from a tridimensional network of BO_6 octahedra sharing all their corners, which is the "backbone" of the structure; this network leaves tunnels parallel to the six directions (1 1 0). Large 8b-centered

cages are formed by the intersection of six tunnels; they can accommodate the O′ species (e.g., extra oxide anions or zeolitic water molecules), the *A* ions being located in 16*d* positions between two adjacent cages, in a (2O′ + 6O) puckered hexagonal bipyramid.

The structural study of the series $Tl_2Nb_2O_{6+x}$ was undertaken from X-ray powder diffraction patterns. The final refinements were made by using a Rietveld program adapted to X-ray data (11).

As noticed previously, all the patterns are indexed with a cubic unit cell and reveal the *Fd3m* space group. A careful examination indicates that some weak lines, 4 4 2, 4 4 6, 8 4 2, 4 4 10-8 8 2, corresponding to the condition *h k l* with $h = 4n$, $k = 4n$, and $l = 2n$, are unambiguously present in the patterns of the composition range $0 < x < 0.5$ (Fig. 3). The presence of these lines indicates that some heavy atoms are located in different positions (32*e*, 96*g*, 96*h*, or 192*i*) than those constituting the classical $A_2B_2O_6O'$ model. So in this composition range, we chose an adapted model from that found by Ganne and Tournoux (12) in the determination of the structure, from single-crystal diffraction data, of the tantalum homologue $Tl_2Ta_2O_6$; here Tl^+ and Tl^{3+} ions are thought to be distributed statistically on half of the 32*e* positions (u, u, u) close to the 16*d* ones—very near to ($\frac{1}{2}$, $\frac{1}{2}$, $\frac{1}{2}$)—Nb in 16*c* (0, 0, 0), O in 48*f* (v, $\frac{1}{8}$, $\frac{1}{8}$), and extra oxide ions O′ in the 8*b* positions ($\frac{3}{8}$, $\frac{3}{8}$, $\frac{3}{8}$) at the centers of the cages previously described. Table 1 summarizes the conditions for the structural determination. For O and O′, the *B* factor is kept fixed at the same value owing to the low electron number of O′ relative to the total electron number. Figure 4 presents the agreement between observed and calculated powder diffraction patterns for $Tl_2Nb_2O_{6.07}$, while Table 2 gathers atomic coordinates and thermal parameters. Four samples in the composition range $0 < x < 0.5$ were studied. Figure 5 shows the evolution of the atomic coordinate of the Tl ions in 32*e* positions (u, u, u) versus composition: it can be seen that Tl ions move toward the 16*d* positions when oxidation occurs, implying the rapid vanishing of the diffraction lines characterized by the condition $h = 4n$, $k = 4n$, $l = 2n$ for a composition close to $x = 0.5$.

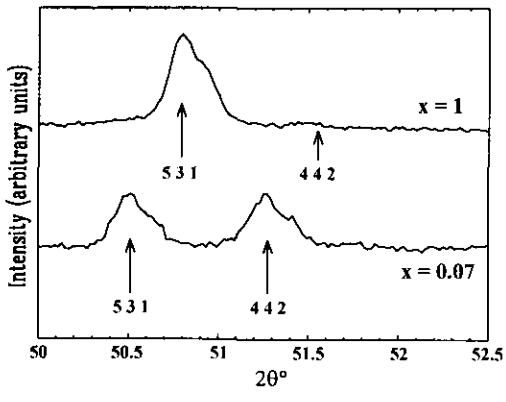

FIG. 3. Part of observed powder diffraction patterns in the region of the 4 4 2 line for $x = 0.07$ and 1.

TABLE 1
Conditions for the Structure Determination and Rietveld Refinement for $Tl_2Nb_2O_{6+x}$ ($x = 0.07$, 0.43, and 1.0)

	$x = 0.07$	$x = 0.43$	$x = 1.0$
Space group	*Fd3m*	*Fd3m*	*Fd3m*
Cell parameter (Å)	10.6829 (2)	10.6399 (2)	10.6220 (2)
Volume (Å^3)	1219.18 (8)	1204.53 (6)	1198.46 (8)
Z	8	8	8
2θ range (°)	10–130	10–130	10–130
Step scan (° 2θ)	0.02	0.04	0.02
Time/step (sec)	28	17	28
Number of *hkl*	78	78	78
Total parameters	16	16	15
x, *y*, *z* coordinates	2	2	1
Thermal parameters	3	3	3
Zero point (°2θ)	0.164 (3)	0.031 (1)	0.097 (2)
	Profile parameters		
*u*1	0.116 (7)	0.189 (8)	0.118 (10)
*v*1	−0.124 (9)	−0.18 (1)	−0.03 (13)
*w*1	0.133 (3)	0.142 (3)	0.119 (4)
*u*2	0.05 (3)	−0.17 (2)	0.11 (3)
*v*2	−0.483 (5)	0.114 (5)	−0.25 (5)
*w*2	1.80 (1)	1.32 (1)	1.40 (2)
C	−0.214 (2)	−0.102 (2)	−0.099 (2)
D	−0.381 (6)	−0.202 (6)	−0.019 (7)
	Discrepancy factors		
R_I	0.0414	0.0330	0.0593
Rp	0.1101	0.0821	0.1163
R_{wp}	0.1287	0.0983	0.1386
R_E	0.0385	0.0386	0.0381

In the range $0.5 < x < 1$, the previous structural model is kept for all the atoms except for Tl ions which are strictly located in the 16*d* positions. Figure 6 shows the agreement between observed and calculated powder diffraction patterns for a composition close to $Tl_2Nb_2O_7$, while Table 2 gives the atomic coordinates and thermal parameters.

3. DISCUSSION OF THE STRUCTURE

Table 3 reports some selected interatomic distances. The Nb–O distance diminishes significantly when the oxidation rate increases, as shown by the decrease in the v_O atomic coordinate (see Fig. 7) and in the unit cell edge length, with the NbO_6 octahedra becoming slightly more distorted. However, the Nb–O distances remain close to the sum of the Nb^{5+} and O^{2-} ionic radii: 1.99 Å (13).

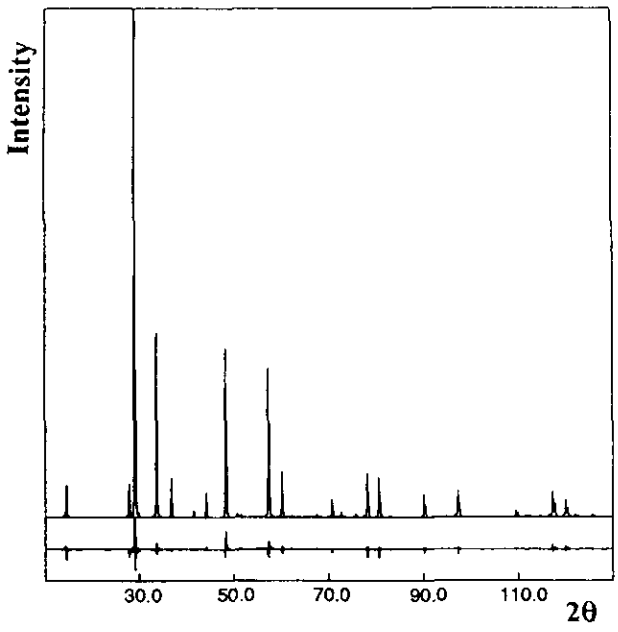

FIG. 4. Comparison between the calculated and observed X-ray diffraction patterns for $x = 0.07$. The difference obs − calc is shown below at the same scale.

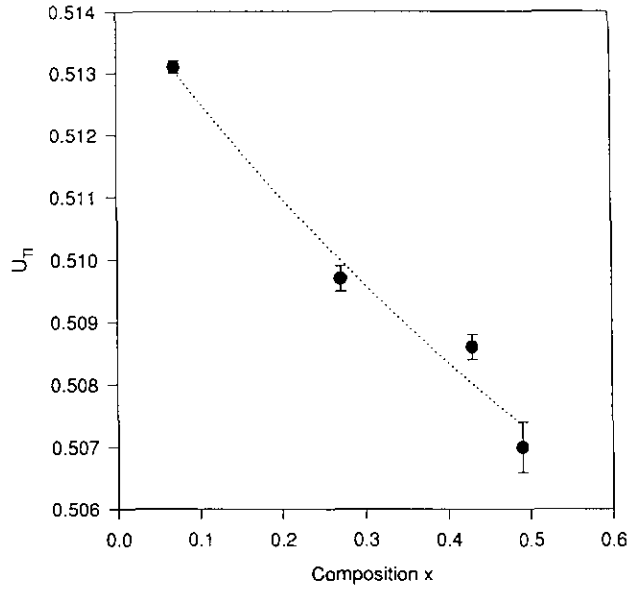

FIG. 5. Evolution of the atomic coordinate u_{Tl} of the Tl ions in 32*e* positions (u, u, u) in the composition range $0 < x < 0.5$. The dotted line is a visual guide.

In the composition range $0 < x < 0.5$, the statistical disorder of Tl^+ and Tl^{3+} in half of the 32*e* positions distorts the classical 2O′ + 6O environment: the 2 Tl–O′ bonds split into a short and a long distance whose difference is reduced as x approaches 0.5, and the 6 Tl–O distances split into two groups presenting slightly different Tl–O bond lengths. The mean Tl–O value remains stable close to 2.700 Å.

When $x > 0.5$, the classical model applies and the Tl–O′ distance stabilizes at the value 2.300 Å, which is significantly shorter than the sum, 2.635 Å, of the average of the Tl^+ and Tl^{3+} (1.285 Å) ionic radii (CN VIII) and of the O^{2-} ionic radius (CN II) (13); the six Tl–O distances enlarge to 2.896 Å, the mean Tl–O distance being 2.75 Å for $x = 1$.

The insertion of x O^{2-} in the 8*b*-centered cages and the correlative oxidation of x Tl^+ into x Tl^{3+} lead to a continuous displacement of the Tl ions from their 32*e* positions toward the 16*d* positions. O′ ions are then tetrahedrally surrounded by Tl ions, the short Tl–O′ distance indicating a marked covalent interaction.

No sign was found for an O′-vacancy ordering as in $Pb_2Ru_2O_{6.5}\square_{0.5}$ and $PbTlNb_2O_{6.5}\square_{0.5}$ (14); neither was one found for a Tl^+–Tl^{3+} ordering.

4. BOND-VALENCE CALCULATIONS

In order to check the validity of the structures and to get some insight into the distribution and position of Tl^I

TABLE 2
Structural Parameters of $Tl_2Nb_2O_{6+x}$

x	0.070	0.271	0.430	0.490	0.588	0.648	1
a(Å)	10.6829(2)	10.6418(2)	10.6399(2)	10.6397(2)	10.6370(2)	10.6313(2)	10.6220(2)
u_{Tl}	0.5131(1)	0.5097(2)	0.5087(2)	0.5070(4)	0.5	0.5	0.5
v_O	0.3035(4)	0.3054(6)	0.3016(5)	0.3013(7)	0.3027(6)	0.2973(7)	0.2925(5)
B_{Tl}(Å^2)	1.46(3)	1.62(5)	1.44(4)	1.27(6)	1.88(3)	2.02(4)	2.71(3)
B_{Nb}(Å^2)	0.29(2)	0.42(3)	0.25(3)	0.21(4)	0.42(3)	0.42(4)	0.23(3)
B_O(Å^2)	0.02(13)	0.39(18)	0.18(16)	−0.7(2)[a]	0.56(2)	1.16(27)	1.6(2)
$B_{O'}$(Å^2)	0.02(13)	0.39(18)	0.18(16)	−0.7(2)[a]	0.56(2)	1.16(27)	1.6(2)

[a] Holding this parameter fixed to a positive value of 0.2 Å^2 does not change significantly the refined value of the other parameters.

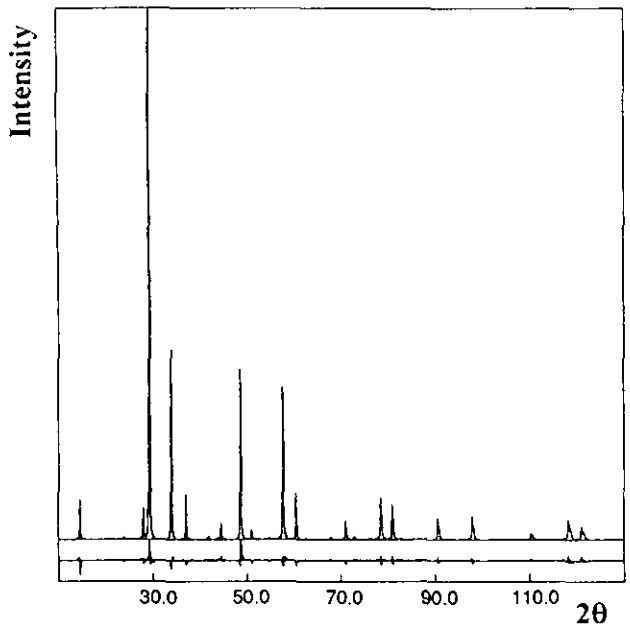

FIG. 6. Comparison between the calculated and observed X-ray diffraction patterns for $x = 1$. The difference is shown below at the same scale.

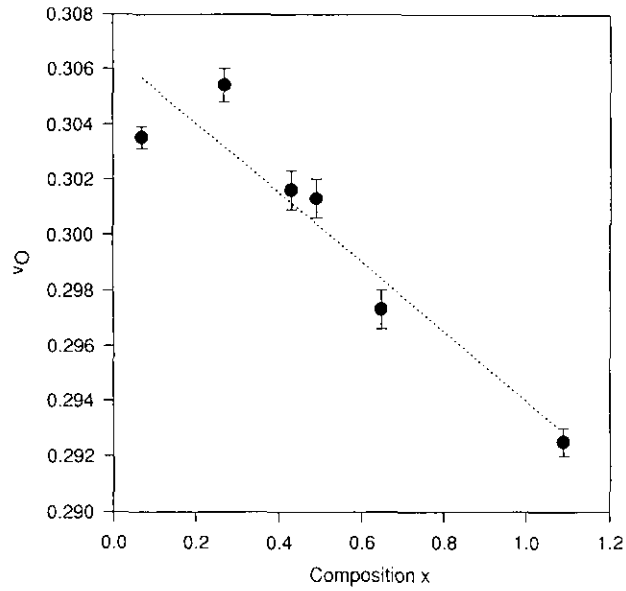

FIG. 7. Evolution of the atomic coordinate v_O of the O anions in 48*f* positions (v, 1/8, 1/8) versus composition. The dotted line is a visual guide.

and Tl^{III}, we carried out a series of bond-valence calculations based on the results presented in the previous section.

The valences were calculated from the formula $\exp[(R - d)/0.37]$, where d is the cation–oxygen distance (Å) and R is the bond-valence parameter tabulated in (15) for the corresponding cations, namely $R = 1.911$ Å, 2.003 Å, and 2.172 Å for Nb^V, Tl^{III}, and Tl^I, respectively.

Niobium Valence

The niobium valences calculated by considering nearest oxygen neighbors are given in Table 4. The valence is close to +5 for low x values, but departs significantly from this value when x increases, as a consequence of the decrease in the Nb–O distances. This might result from an inaccuracy in the oxygen position, or from the existence of some bond strain in the structure (see (16)). An alternate origin might be the emergence of a certain degree of covalence between oxygen and thallium as oxygen content increases. Such a possibility will be considered later on. It would slightly decrease the effective negative charge on oxygen anions, which could not be considered as purely ionic −2 centers any longer. The Nb–O bond strength would thus be slightly reduced, with a correlatively more reasonable Nb valence at high oxygen content.

Correlation between Thallium Position and Valence

As mentioned in Section 2, one structural feature of the oxidation of $Tl_2Nb_2O_6$ is the progressive decrease of the splitting of Tl on 32*e* sites ($u(Tl) > 0.5$), which vanishes for $x > 0.5$ with Tl on 16*d* sites ($u(Tl) = 0.5$). Such behavior appears to be a direct consequence of the introduction

TABLE 3
Selected Interatomic Distances in $Tl_2Nb_2O_{6+x}$ (Å)

x	Nb–O	Tl–O′	Tl–O	⟨Tl–O⟩
0.07	1.973 (3)	2.070 (1) 2.555 (1)	3 × 2.806 (4) 3 × 2.862 (3)	2.704
0.27	1.971 (5)	2.125 (1) 2.483 (1)	3 × 2.782 (3) 3 × 2.825 (4)	2.679
0.43	1.959 (4)	2.143 (2) 2.464 (2)	3 × 2.814 (3) 3 × 2.850 (4)	2.700
0.49	1.959 (4)	2.175 (4) 2.432 (4)	3 × 2.818 (5) 3 × 2.847 (6)	2.700
0.588	1.962 (4)	2.303 (2)	6 × 2.818 (4)	2.689
0.648	1.945 (5)	2.302 (2)	6 × 2.860 (4)	2.720
1.	1.931 (4)	2.300 (1)	6 × 2.896 (4)	2.747

TABLE 4
Cation Valences in $Tl_2Nb_2O_{6+x}$ as a Function of x

x	0.070	0.271	0.430	0.490	0.588	0.648	1
Val(Nb)	5.074	5.102	5.270	5.270	5.227	5.473	5.684
$q(Tl)^a = 1 + x$	1.070	1.271	1.430	1.490	1.588	1.648	2
$Val(Tl)_{Model\ I}$	1.108	1.440	1.538	1.580	1.671	1.629	1.850
$Val(Tl)_{Model\ II}$	1.097	1.308	1.369	1.432	1.664	1.616	1.850

[a] $q(Tl)$ = Formal charge on thallium assuming O^{2-} and Nb^{5+}.

of extra oxygen atoms in the structure framework. Our aim here is to evidence the relevance of such a Tl shift by bond-valence calculations.

$x = 0$. Verbaere *et al.* carried out (17) electrostatic energy calculations on $Tl_2Ta_2O_6$, which is isostructural to $Tl_2Nb_2O_6$, with statistical occupancy of Tl on 32*e* sites as in the latter. They showed, by taking account of thallium polarization, that the interaction energy of thallium with the rest of the structure exhibits a double-well shape as a function of the thallium position parameter u. The minimum of energy corresponds to a parameter u different from 0.5, thus favoring statistical occupancy of sites 32*e* by Tl, rather than full occupancy of sites 16*d*. Following a similar line of thought, but on valence, we carried out calculations of Tl valence in $Tl_2Nb_2O_6$ as a function of the u parameter. Since the preparation of a perfectly stoichiometric $x = 0$ sample has not been possible, cell and oxygen parameters for such an hypothetical compound were deduced by linear extrapolation of the experimental values for $x > 0$ (see (18)). With such values, the calculated thallium valence as a function of u has a concave shape, with maximum at $u = 0.5$ (see Fig. 8a). Such a shape results from the weakening of the Tl–O bond strength due to the increase in Tl–O distances when Tl is moved away from the 16*d* site. The interesting point is that the curve $y = Val(Tl) - q(Tl) = f(u)$, where $q(Tl)$ is the formal charge of thallium ($q = 1 + x$) cuts the axis $y = 0$ for values of u different from 0.5, namely $u = 0.525$. This value is comparable to the observed value for $x = 0.07$ ($u = 0.513$) or from the value extrapolated from experimental points for $x = 0$ ($u \approx 0.515$). Therefore, it can be concluded that a shifting of Tl away from the 16*d* position is in agreement with an optimization of its valence. In the following, we will try to extend such conclusions to the case $x > 0$.

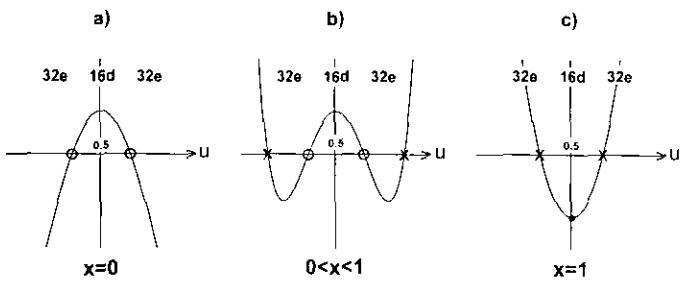

FIG. 8. Qualitative evolution with x of the curve $Val(Tl) - (1 + x) = f(u)$. The curve crosses the horizontal axis at a point (marked by open circles or crosses) representing the theoretical position u of thallium, where its calculated valence equals its formal charge (see also Fig. 9 for the relative position of Tl and oxygen O').

$x > 0$, Model I. The introduction of oxygen O' into the structure drastically modifies the shape of the valence curve, since shifting Tl away from $u = 0.5$ on a 32*e* position moves it toward the O' position. When the compound is fully oxidized ($x = 1$), there results an inversion of the concavity of the curve, which becomes convex with a minimum at $u = 0.5$ (see Fig. 8c). In between these two extremes, for some values of x between 0 and 1, a more complex, double-welled shape is observed (Fig. 8b). If such a curve crosses the $y = 0$ axis at four distinct points (marked by circles and crosses in Fig. 8b), this means that two values of the parameter u are compatible with Tl valence. Another criterion, most likely electrostatic repulsion, is necessary to select one of these two values. For instance, by considering the Tl atomic configuration around oxygen O', which forms a tetrahedron, it can be seen that shifting it too far away from the $u = 0.5$ position (corner of the tetrahedron on Fig. 9) would increase the electrostatic repulsion between some Tl atoms, which is less favorable. Therefore, in the following and in the case where two values of u are compatible with Tl valence, we will consider only that which is closer to 0.5, which moreover allows for continuity with the case $x = 0$.

In comparison with the case $x = 0$, a complication arises from the fact that Tl^{I} is partially substituted by Tl^{III} on site 32*e*, and that oxygen O' only partially occupies site 8*b*. The simplest assumption is to consider that Tl^{I} and Tl^{III} are randomly distributed on site 32*e*, independent of the random occupation of site 8*b* by oxygen O'. This will be called Model I. As in the case $x = 0$, linear extrapolations from experimental data are used for cell parameter a and oxygen position parameter v (18) in order to remedy the dispersion of experimental points.

Assuming that the compound is purely ionic, its formula

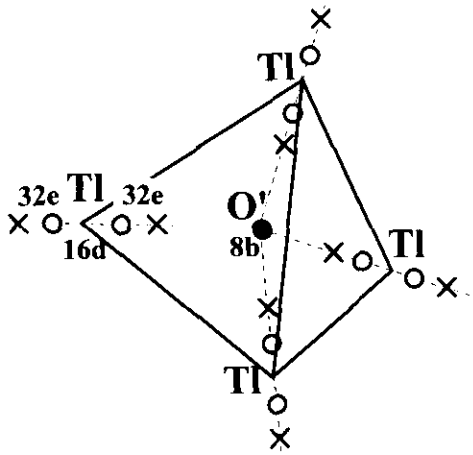

FIG. 9. Tetrahedral configuration of Tl atoms surrounding an oxygen O'. The tetrahedron corners correspond to sites 16*d*. Open circles and crosses represent sites 32*e* for two different values of position parameter *u* (see also Fig. 8).

can be written $Tl^{I}_{2-x}\,Tl^{III}_{x}\,Nb^{V}_{2}\,O_6\,O'_x$. Each Tl atom is surrounded by 6 oxygens O and $2x$ oxygens O' on average. If u(Tl) is different from 0.5, half the thallium-oxygen distances are shorter than the other half; short and long thallium-oxygen distances will be called S and L for oxygen O, and s and l for oxygen O', respectively. In Model I, the mean valence of Tl is thus computed for the following average distribution of distances:

$3S + 3L + xs + xl$, with $(2 - x)Tl^{I}$ and xTl^{III} (see Fig. 10a).

The evolution of Tl valence with parameter u according to this model has been calculated for different values of x, and some representative curves Val(Tl) $-$ $(1 + x)$ as a function of u are presented in Fig. 11a. For a given value of x, the theoretical value of parameter u is given by the intersection of the curve with axis $y = 0$. The evolution with x of theoretical and experimental values of u is presented on Fig. 12a. It can be seen that the theoretical results depart dramatically from the experimental values. This is strong evidence that the basic assumptions of Model I are wrong.

$x > 0$, Model II. The central hypothesis of Model I assumes a random occupation of 32*e* sites and 8*b* sites by Tl^{III} and oxygen O', respectively, with no correlation. Such an assumption must be questioned. For a more realistic model, some hints can be found by considering the valence of oxygen O'. As mentioned earlier, oxygen O' is surrounded by four Tl atoms. In the low oxygen range ($x < 0.5$) thallium randomly occupies 32*e* sites, which means that whatever the thallium valence, the two types of Tl–O' distances, long (l) or short (s), coexist. One can assess what would be the most favorable configuration implying Tl^{I} and Tl^{III} around oxygen O' by calculating the O' valence for all possible combinations of short and long distances: the most likely configuration would be that giving a value closest to 2. Since there is some doubt as to the fully ionic character of Tl and O at high oxygen content, we will limit ourselves to the low oxidation range, $x < 0.5$, which implies that there is less than one Tl^{III} for three Tl^{I} in the compounds. We will thus consider only those situations where either four Tl^{I} or one Tl^{III} and three Tl^{I} surround oxygen O'. Table 5 lists all the corresponding possibilities and the associated valences for oxygen O'

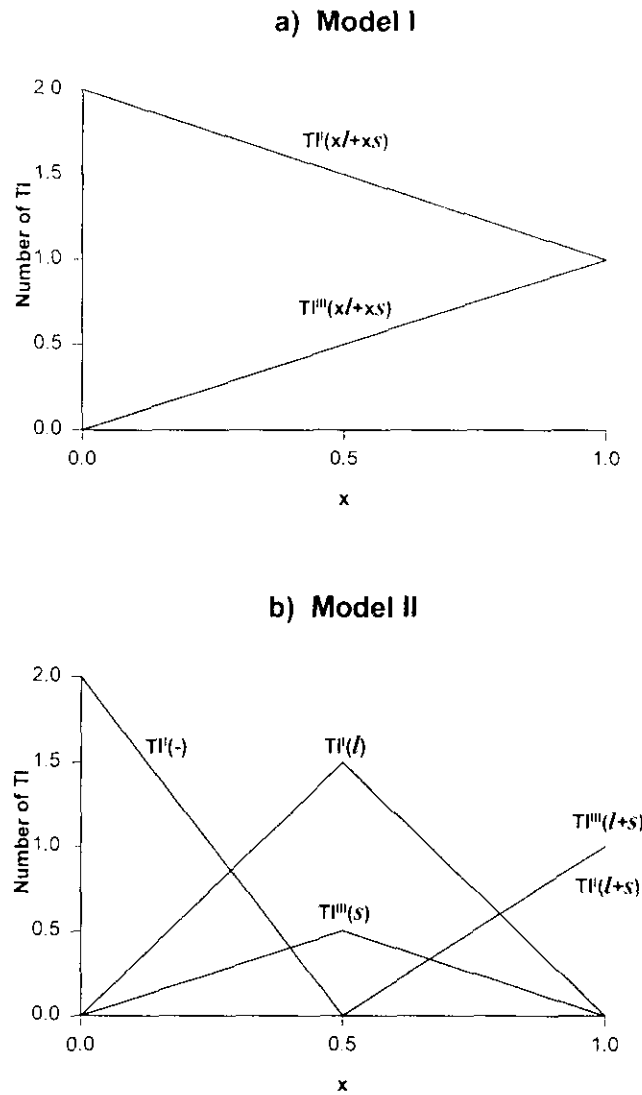

FIG. 10. Evolution with x of the balance between Tl^{I} and Tl^{III} according to their surroundings (a) Model I: statistical hypothesis; (b) Model II: imposing one short Tl^{III}–O' and three long Tl^{I}–O' distances around each oxygen O' at low oxidation ($x < 0.5$).

The letters s and l in parentheses refer to short and long Tl–O' distances, respectively.

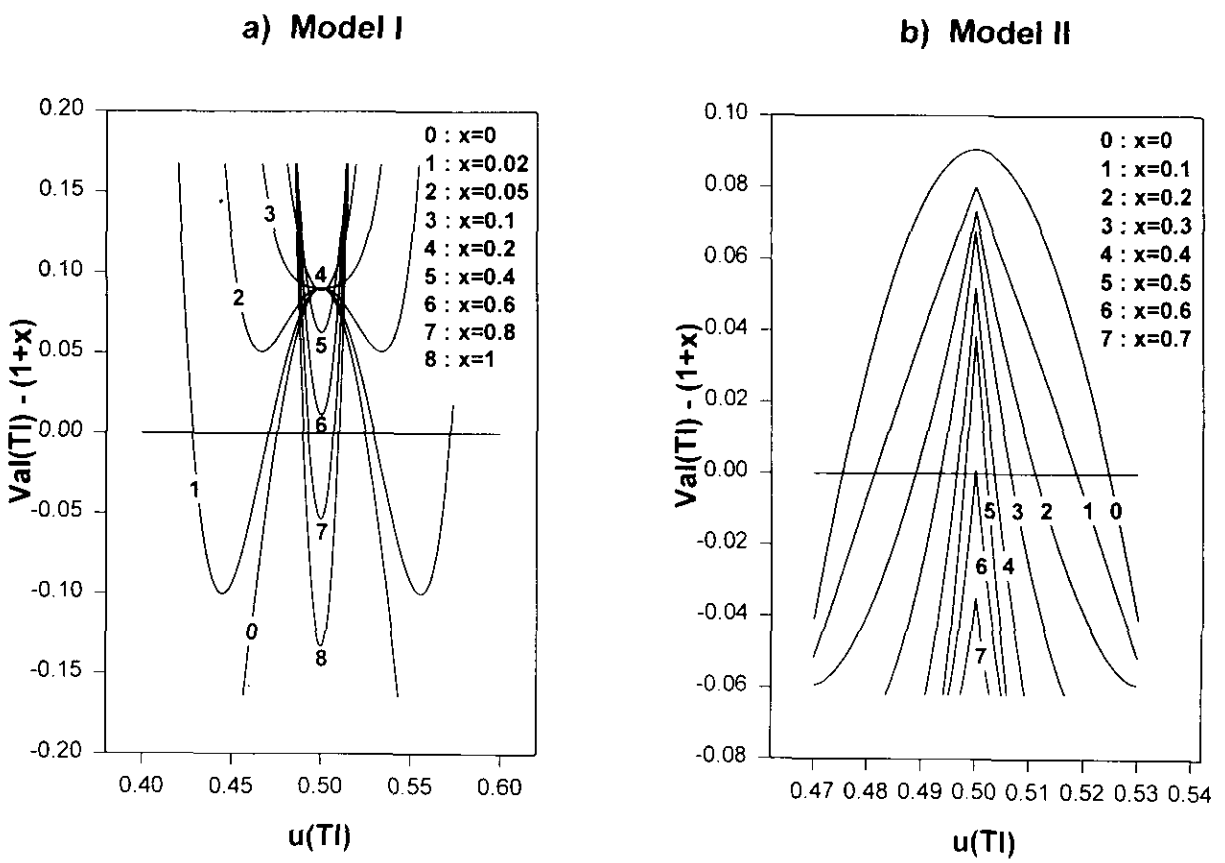

FIG. 11. The Tl valence curves Val(Tl) − (1 + x) as a function of the u(Tl) position parameter, for different values of x, in the cases of Model I and Model II.

for each of the studied compounds with $x < 0.5$. Clearly the most probable configuration around oxygen O′ is $s_3 l_1^3$, that is, one trivalent Tl with short Tl^{III}–O′ distance and three monovalent Tl with long Tl^{I}–O′ distances. Since there are as many oxygens O′ as Tl^{III} in the compound (x), the picture which emerges does not support a random distribution of Tl^{III} relative to O′: it is as if any time an extra oxygen O′ is introduced in the structure, it attracts one of its four Tl neighbors, which becomes trivalent, and repels the three remaining monovalent Tl.

Model II has been designed according to this scheme. Figure 10b gives the evolution with x of Tl^{I} and Tl^{III} surroundings adopted in this model. Although it appears to be slightly more complex than model I (Fig. 10a), it is still a simplistic model, since it assumes linear variation with x of all the quantities, and is only deduced from the most probable surroundings of oxygen O′. Within such a model, $x = 0.5$ is a singular point, above which there is no more 6-coordinated thallium, and 8-coordinated Tl appears. Above $x = 0.5$, linear evolution is postulated up to $x = 1$, the limit where only 8-coordinated Tl subsist, as in any stoichiometric pyrochlore structure. The oversimplification of the model also appears from the fact that, for $x = 0.5$, it would imply perfect O′-vacancy and Tl orders, which is apparently not the case since no superstructure is observed. However, such a model shows better agreement with expected thallium valence than Model I, as can be seen in Table 4: the discrepancy is within 4.5% for $x < 0.5$, and within 7.5% for $x > 0.5$. This gives confidence that such a model is more realistic than Model I, which we checked by calculating the evolution of u(Tl) as a function of x. Since, as in the case of Model I, the valence curves exhibit, for some values of x, a double-well structure, we only considered those u(Tl) values closest to 0.5 for the same reasons as given previously.

Figure 11b gives the evolution of the valence curve Val(Tl) − (1 + x) as a function of u for different values of x, with the point where it crosses the axis $y = 0$ reported in Fig. 12b (line) as the calculated u position of Tl according to Model II. There is now an almost quantitative agreement with the observed values, with a progressive attenuation of the splitting of Tl, which disappears at $x = 0.5$ as effectively observed. The slight departure which remains probably results from the roughness of the linear model. Above $x = 0.5$, the valence of Tl for $u = 0.5$ is lower than the expected value, and the difference

increases when x increases up to $x = 1$, for which the valence calculations do not depend on any postulated model. It is to be noted that, for $x > 0.5$, a solution exists with $u > 0.5$, which corresponds to the external convex part of the curve (see Fig. 8c), but it is not selected, perhaps because of electrostatic repulsion between Tl as mentioned above, since the charge on Tl increases with x. The difference between expected and measured valence might be due to a certain degree of covalence between thallium and oxygen, which would lower the effective charge on each ion by delocalizing electrons. This is to be correlated with the effect observed on Nb valence and described earlier. However, an inaccuracy on the position of oxygen O cannot be ruled out, although it is difficult to imagine why it would affect mostly the strongly oxidized samples, increasing with x. Neutron diffraction experiments would be necessary to clarify this point.

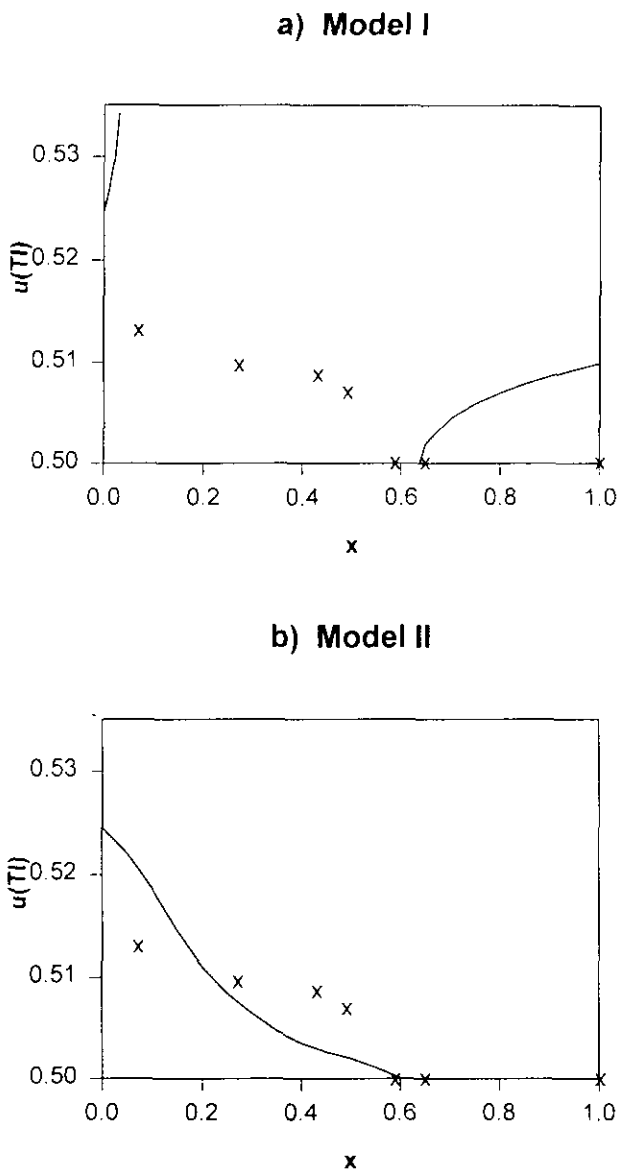

FIG. 12. Evolution with x of the position parameter u of thallium as effectively observed (crosses) and calculated from Models I and II (full lines).

TABLE 5
'Oxygen O' Valence in $Tl_2Nb_2O_{6+x}$ Depending on the Surrounding Configuration[a]

x	0.070	0.271	0.430	0.490
s_1^4	5.264	4.540	4.324	3.972
$s_1^3 l_1$	4.303	3.837	3.697	3.473
$s_1^2 l_1^2$	3.342	3.134	3.070	2.974
$s_1 l_1^3$	2.381	2.431	2.443	2.475
l_1^4	1.420	1.728	1.816	1.976
$s_3 s_1^3$	4.781	4.124	3.927	3.608
$s_3 s_1^2 l_1$	3.810	3.421	3.300	3.109
$s_3 s_1 l_1^2$	2.859	2.718	2.673	2.610
$\mathbf{s_3 l_1^3}$	**1.898**	**2.015**	**2.046**	**2.111**
$l_3 s_1^3$	4.173	3.678	3.531	3.292
$l_3 s_1^2 l_1$	3.212	2.975	2.904	2.793
$l_3 s_1 l_1^2$	2.251	2.272	2.277	2.294
$l_3 l_1^3$	1.290	1.569	1.650	1.795

[a] s and l refer to short and long Tl–O' distances, respectively. The indices represent the oxidation state of thallium (+1 or +3) and the exponents count the number of corresponding distance in oxygen O' surrounding (the sum of all exponents for a given configuration is thus always 4).

CONCLUSION

The oxidation of $Tl_2Nb_2O_6$ produces a continuous solid solution $Tl_2Nb_2O_{6+x}$; the cubic pyrochlore structural type is maintained. The correlative insertion of x O^{2-} anions and the oxidation of x Tl^+ into x Tl^{3+} leads to the contraction of the unit cell edge, to the displacement of the Tl ions toward the 16*d* positions, and to the creation of short Tl–O' distances. It has been possible to deduce some correlation between oxygen insertion and the distribution of Tl^{III} in $Tl_2Nb_2O_{6+x}$ from valence calculations. Each time an extra oxygen O' is introduced in the lattice, one Tl closest neighbor is oxidized to +3. Assuming such a model, valence calculations are in good agreement with the splitting of Tl on site 32*e* ($u > 0.5$) and with the decrease of this splitting when x increases up to 0.5 ($u = 0.5$, site 16*d*). For x greater than 0.5, valence calculations suggest a certain degree of covalence between Tl and O, or an inaccuracy in the oxygen position. Some further work is needed to explore the physical properties of these materials.

ACKNOWLEDGMENTS

We are indebted to Dr. Retoux, who performed the thermodiffractometry experiments. We also thank Professor Ferey for the acquisition

of the oxygen pressure vessel and Mr. Olsztynski for his help with the installation of the high pressure experiment.

REFERENCES

1. K. S. Vorres, "Amer. Ceram. Soc., Abstract of papers," 42-0, 1964.
2. I. N. Belyaev, D. S. Lesnykh, and T. G. Lupeiko, *Russ. J. Inorg. Chem. Engl. Transl.* **3,** 338 (1969).
3. I. N. Belyaev, D. S. Lesnykh, and T. G. Lupeiko, *Russ. J. Inorg. Chem. Engl. Transl.* **15,** 198 (1970).
4. N. Ramadass, T. Palanisami, J. Gopalakrishnan, G. Aravamudan, and M. V. C. Sastri, *Solid State Commun.* **17,** 545 (1975).
5. C. Michel, Thèse de Doctorat de Spécialité Caen 1974.
6. A. W. Sleight, *Mater. Res. Bull.* **4,** 377 (1969).
7. J. M. Longo, P. M. Raccah, and J. B. Goodenough, *Mater. Res. Bull.* **4,** 191 (1969).
8. J. M. Longo, P. M. Raccah, J. A. Kafalas, and J. W. Pierce, *Mater. Res. Bull.* **7,** 137 (1972).
9. H. S. Jarrett, A. W. Sleight, J. F. Weiher, J. L. Gillson, C. G. Frederick, G. A. Jones, R. S. Swingle, D. Swartzfager, J. E. Gulley, and P. C. Hoell, *in* "Valence Instabilities and Related Narrow-Band Phenomena" (R. D. Parks, Ed.), p. 545. Plenum, New York, 1977.
10. H. S. Horowitz, J. M. Longo, and J. T. Lewandowski, *Mater. Res. Bull.* **16,** 489 (1981).
11. A. Le Bail, unpublished program; and A. Le Bail, H. Duroy, and J. L. Fourquet, *Mater. Res. Bull.* **23,** 447 (1988).
12. M. Ganne and M. Tournoux, *Mater. Res. Bull.* **10,** 1313 (1975).
13. R. D. Shannon, *Acta Crystallogr. Sect. A* **32,** 751 (1976).
14. R. A. Beyerlein, H. S. Horowitz, J. M. Longo, and M. E. Leonowicz, *J. Solid State Chem.* **51,** 253 (1984).
15. N. E. Brese and M. O'Keefe, *Acta Crystallogr. Sect. B* **47,** 192 (1991).
16. I. D. Brown, *Acta Crystallogr. Sect. B* **48,** 553 (1992).
17. A. Verbaere, M. Ganne, and M. Tournoux, *J. Solid State Chem.* **31,** 47 (1980).
18. The evolution of crystallographic parameters with x was deduced from Figs. 1 and 2 to be as follows:

    a (Å) = 10.6964 − 0.1837x, for $x < 0.28$; and a (Å) = 10.6512 − 0.0242x, for $x > 0.28$; v_o = 0.3066 − 0.01257x.